Fundamental J. Thermal Science and Engineering, Vol. 2, Issue 1, 2012, Pages 13-36
Published online at http://www.frdint.com/

PERTURBATION ANALYSIS OF DISSIPATION AND THERMAL RADIATION EFFECTS ON HYDROMAGNETIC TRANSIENT MIXED CONVECTIVE HEAT AND MASS TRANSFER WITH TRANSPIRATION

SAHIN AHMED[1], OSMAN ANWAR BÉG[2], SEYEDALI VEDAD[3], NILOOFAR HEIDARI[3], MEHRNOOSH ZEINALKHANI[3], MOHAMMADALI GHORBANI[3] and ALIREZA HEIDARI[3,*]

[1]Fluid Mechanics Research
Department of Mathematics
Goalpara College
Goalpara-783101, Assam, India

[2]Magnetohydrodynamics, Aerodynamics and Heat Transfer Research
Department of Engineering and Mathematics
Sheffield Hallam University
Sheffield, South Yorkshire, S11WB, UK

[3]Institute for Advanced Studies
Tehran 14456-63543, Iran
e-mail- Prof.Alireza.Heidari@InstituteforAdvancedStudies.us

Abstract

We investigate theoretically the unsteady magnetohydrodynamic natural convection heat and mass transfer of a viscous, incompressible, electrically-conducting and radiating fluid over a porous vertical infinite plate. A uniform magnetic field of magnitude B_0 is applied normal to the

Keywords and phrases: magnetohydrodynamics, thermal radiation, mixed convection, wall suction, heat transfer, mass transfer, viscous dissipation, magnetic materials processing, perturbation solutions, unsteady.

*Corresponding author

Received January 11, 2012

plate. An algebraic flux model is employed valid in the optically thin limit to simulate radiative heat transfer. Magnetic induction effects are excluded. However viscous heating and wall transpiration effects are included in the model. Following non-dimensionalization of the transient boundary layer conservation equations, a perturbative series expansion solution is derived. Expressions are also obtained for the surface shear stress (skin friction), Nusselt number and Sherwood number. An increase in magnetic body force parameter (M) is found to escalate temperatures in the regime whereas an increase in the conduction-radiation parameter (R) is shown to exert the opposite effect. Velocity is reduced considerably with a rise in conduction-radiation parameter (R) whereas the temperature is found to be markedly boosted with an increase in the viscous dissipation effect, i.e., Eckert number. Velocity and concentration functions are both reduced with an increase in Schmidt number. Similarly velocity and temperature are both considerably decreased with an increase in the free convection parameter, i.e., Grashof number.

1. Introduction

Transport phenomena in materials processing flows in the presence of magnetic fields have stimulated considerable attention in recent years. Many modern technologies involve the interaction of electromagnetic fields and flowing liquids such as metal production and electrolytic manufacture. Magnetic damping involves the application of an intense, static magnetic field to suppress fluid motion. Semiconductors, smart metallic alloys, ceramics and intelligent metallo-organic liquids are often produced using electromagnetic materials processing as are ferrofluids for medical applications, laser welds, nano-scale metallic powders etc. [1-3]. Important magneto-fluid dynamic phenomena arising in materials processing including the flow of metal along translating surfaces, magnetic-field control in the production of steel, aluminum, and high-performance superalloys and also magnetic stirring, where a rotating magnetic field is used to agitate and homogenize the liquid zone of a partially-solidified ingot [4]. Applications of magnetohydrodynamic boundary layer flows in crystal growth processes are also significant [5]. When magnetohydrodynamic flows are combined with simultaneous heat and species diffusion under free convection, the resulting multi-physical flow phenomena are characterized by numerous intricate interactions. Buoyancy-driven transport processes also occur in geophysics and such flows are modified or driven by density differences caused by temperature, chemical composition differences and gradients, and material or phase constitution. Elucidation of the multiple effects arising in such flow regimes such as the interplay between thermal and concentration buoyancies is necessary to successfully control these processes, particularly in an industrial context. Regimes are further complicated by the presence of unsteadiness, i.e., transient phenomena. Steady and unsteady combined heat and mass transfer by free convection along an infinite and semi-infinite vertical plate have been studied extensively by different scholars. Much of the work reported up to 1988 has been addressed lucidly by Gebhart et al. [6]. Several excellent studies of both steady and transient hydromagnetic convection flows have been communicated, using a variety of analytical and numerical methods. Soundalgekar [7] investigated analytically the two-dimensional steady hydromagnetic flat plate flow with constant suction velocity for the case of both plate cooling and heating and with viscous heating present. Krishna and Prasada Rao [8] used complex variables to study Hall effects on the rotating hydromagnetic thermal boundary layers along an infinite oscillatory porous plate under a uniform transverse magnetic field. Hossain and Mandal [9] presented numerical solutions for transient laminar free convection hydromagnetic flow along an accelerated vertical infinite porous plate with wall suction velocity proportional to $(\text{time})^{-1/2}$ for both water and air. Kafoussias [10] used a Laplace transform method to study Soret effects on hydromagnetic free-convective heat and mass transfer along a translating vertical infinite plate, for both cases of the impulsively started and uniformly accelerated plate. Sattar [11] considered Hall current effects on unsteady magneto-convective flow under an oblique magnetic field. Acharya et al. [12] reported on transient hydromagnetic flow caused by the interaction of gravity and density difference due to simultaneous diffusion of thermal energy and chemical species with Hall currents. Nanousis [13] studied plate oscillation influence on hydromagnetic thermal boundary layer flow along a porous plate, also solving the magnetic induction equations and including dissipation effects.

Coupled heat and mass transfer in hydromagnetic flows are also of considerable interest. In particular with buoyancy forces present, free convection effects can exert a major role in such regimes. Char [14] presented closed-form solutions for the combined heat and mass transfer in a hydromagnetic flow of a viscoelastic fluid along a stretching surface, showing that increasing magnetic field elevates both temperature and species concentration increase whereas the mass transfer coefficient at the wall is reduced with a decrease in modified Schmidt number decreases. Rawat et al. [15] used the finite element method to simulate the unsteady hydromagnetic natural convection heat and mass transfer in a non-Darcian porous medium channel for the case of an electrically-conducting micropolar fluid. Zueco et al. [16]

employed the network simulation method to study thermophoretic effects on magnetohydrodynamic heat and mass transfer in boundary layer flow along a flat plate with viscous heating, Joule heating and wall suction. These studies all identified the strong influence of transverse magnetic field on very different flow regimes.

In numerous high-temperature materials processing operations, conduction and convection heat transfer are invariably accompanied with thermal radiation heat transfer. Radiation may have a dominant role in, for example, Czochralski crystal growth processes [17]. It has been shown that thermal radiation is among the best mechanisms for rapid thermal processing (RTP) and rapid thermal chemical vapor deposition (RTCVD) of semiconductor wafers [18]. Other important areas in which thermal radiation heat transfer must be considered with thermal convection heat transfer (and mass transfer) are direct flame impingement (DFI) furnace for rapid heating of metals in materials processing [19], heating of a continuously moving load in the industrial radiant oven [20] and glass melting simulation [21]. Several articles have addressed the combined effects of thermal radiation and magnetohydrodynamic phenomena on combined heat and species transfer flows. A significant drawback of modeling thermal radiation effects is a robust solution of the radiative transfer integro-differential equation [22]. To circumvent this, generally simplified algebraic flux models such as the two-flux model, Milne-Eddington approximation or the Rossel and diffusion approximation, are employed in engineering studies owing to their adaptability to boundary layer heat transfer models. Shateyi and Petersen [23] used the Rosseland flux model to examine numerically the influence of thermal radiation and buoyancy effects on heat and mass transfer over a semi-infinite stretching surface with wall flux effects, showing thermal radiation flux exerts a strong effect on the regime. Ogulu and Prakash [24] employed the optically-thin Milne-Eddington differential radiation approximation to study analytically the hydromagnetic convection flow along a moving plate with viscous dissipation effects. Further interesting studies of radiative-convective magnetohydrodynamic flows in a variety of applications have been communicated in [25-32]. In several of these studies viscous dissipation effects have also been considered.

In the present analysis, we investigate theoretically thermal radiation heat transfer effects on an unsteady two-dimensional laminar mixed convective thermal and species boundary layers along an accelerated semi-infinite vertical permeable plate with variable suction, in the presence of a transverse magnetic field. Viscous dissipation effects are included. Such a study has thus far not been communicated in the engineering science or applied mathematics literature and finds pertinent applications in high-temperature magneto materials processing.

2. Mathematical Model

We study the transient magneto hydrodynamic free convection heat and mass transfer in viscous, incompressible, Newtonian, electrically-conducting flow of a radiating fluid over a porous vertical infinite plate. Thermal and concentration buoyancy effects are present owing to free (natural) convection effects. The physical regime is illustrated in figure below.

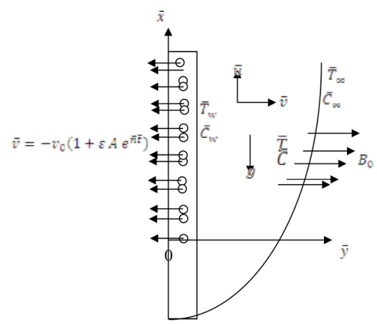

The $\bar{x}$-axis is assumed to be taken along the plate and the $\bar{y}$-axis normal to the plate. The plate is considered infinite in the $\bar{x}$-direction and therefore all physical quantities will be independent of $\bar{x}$. Under these assumptions, the physical variables are functions of $\bar{y}$ and $\bar{t}$ only. The wall is maintained at constant temperature $\overline{T}_w$ and concentration $\overline{C}_w$ higher than the ambient temperature $\overline{T}_\infty$ and concentration $\overline{C}_\infty$, respectively. A uniform magnetic field of magnitude B_0 is applied normal to the plate. The transverse magnetic field and magnetic Reynolds number are assumed to be sufficiently weak, so that the induced magnetic field is negligible. Also there is no applied voltage indicating that electric field is absent. The concentration of the diffusing species in the binary mixture is assumed to be very small in comparison with the other chemical species, which are present, and hence Soret and Dufour effects are negligible. A unidirectional thermal radiation flux is present perpendicular to the plate. Under the Boussinesq approximation and boundary layer theory, the governing equations for the problem under consideration are:

$$\frac{\partial \bar{v}}{\partial \bar{y}} = 0, \tag{1}$$

$$\frac{\partial \bar{u}}{\partial \bar{t}} + \bar{v}\frac{\partial \bar{u}}{\partial \bar{y}} = -\frac{1}{\rho}\frac{\partial \bar{p}}{\partial \bar{x}} + \upsilon \frac{\partial^2 \bar{u}}{\partial \bar{y}^2} + g\,\beta(\bar{T} - \bar{T}_\infty) + g\bar{\beta}(\bar{C} - \bar{C}_\infty) - \frac{\sigma B_0^2}{\rho}\bar{u}, \quad (2)$$

$$\frac{\partial \bar{T}}{\partial \bar{t}} + \bar{v}\frac{\partial \bar{T}}{\partial \bar{y}} = \frac{\kappa}{\rho C_P}\left[\frac{\partial^2 \bar{T}}{\partial \bar{y}^2} - \frac{1}{k}\frac{\partial \bar{q}}{\partial \bar{y}}\right] + \frac{\upsilon}{C_P}\left(\frac{\partial \bar{u}}{\partial \bar{y}}\right)^2, \quad (3)$$

$$\frac{\partial^2 \bar{q}}{\partial \bar{y}^2} - 3\alpha^2 \bar{q} - 16\sigma^* \alpha \bar{T}^3{}_\infty \frac{\partial \bar{T}}{\partial \bar{y}} = 0, \quad (4)$$

$$\frac{\partial \bar{C}}{\partial \bar{t}} + \bar{v}\frac{\partial \bar{C}}{\partial \bar{y}} = D\frac{\partial^2 \bar{C}}{\partial \bar{y}^2}. \quad (5)$$

The third and fourth terms on the right hand side of the momentum equation (2) denote the thermal and concentration buoyancy effects, respectively. Also the second and third terms on the right hand side of the energy equation (3) represent the radiative heat flux and viscous dissipation effects, respectively. Equation (4) represents the Milne-Eddington differential approximation for radiation which yields quite good accuracy for boundary layer flows [33]. The corresponding boundary conditions of the problem are:

$$\left.\begin{aligned} &\bar{u} = \bar{u}_P,\ \bar{T} = \bar{T}_w + (\bar{T}_w - \bar{T}_\infty)e^{\bar{n}\bar{t}},\ \bar{C} = \bar{C}_w + (\bar{C}_w - \bar{C}_\infty)e^{\bar{n}\bar{t}} \ \text{at}\ \bar{y} = 0, \\ &\bar{u} \to \bar{U}_\infty = U_0(1 + \varepsilon e^{\bar{n}\bar{t}}),\ \bar{T} \to \bar{T}_\infty,\ \bar{C} \to \bar{C}_\infty \ \text{as}\ \bar{y} \to \infty. \end{aligned}\right\} \quad (6)$$

In equation (1), it is evident that the suction (transpiration) velocity at the plate is either a constant or function of time only. Hence the suction velocity normal to the plate is assumed to take the form, following Ahmed [34, 35]:

$$\bar{v} = -V_0(1 + \varepsilon A e^{\bar{n}\bar{t}}), \quad (7)$$

where A is a real positive constant and ε is small such that $0 < \varepsilon << 1$, $\varepsilon A << 1$, and $V_0 > 0$, the negative sign indicates that the suction is towards the plate. External to the boundary layer, i.e., in the free stream, equation (3) reduces to:

$$-\frac{1}{\rho}\frac{\partial \bar{p}}{\partial \bar{x}} = \frac{d\bar{U}_\infty}{d\bar{t}} + \frac{\sigma B_0^2}{\rho}\bar{U}_\infty. \quad (8)$$

Since the medium is optically thin with relatively low density and α (absorption coefficient) $<< 1$, the radiative heat flux given by equation (4), following Shateyi et al. [36] takes the algebraic form:

$$\frac{\partial \bar{q}}{\partial \bar{y}} = 4\alpha^2(\bar{T} - \bar{T}_\infty), \tag{9}$$

where $\alpha^2 = \int_0^\infty \delta\lambda \frac{\partial B}{\partial \bar{T}}$ and B is Planck's function. All other parameters have been defined implicitly in the nomenclature. To facilitate a perturbation solution, we introduce the following non-dimensional quantities into the equations (1) to (5):

$$y = \frac{v_0 \bar{y}}{\upsilon}, \quad u = \frac{\bar{u}}{U_0}, \quad v = \frac{\bar{v}}{V_0}, \quad U_\infty = \frac{\bar{U}_\infty}{U_0}, \quad n = \frac{\bar{n}\upsilon}{V_0^2}, \quad t = \frac{\bar{t}V_0^2}{\upsilon},$$

$$\upsilon = \frac{\mu}{\rho}, \quad Ec = \frac{U_0^2}{C_P(\bar{T}_w - \bar{T}_\infty)}, \quad \theta = \frac{\bar{T} - \bar{T}_\infty}{\bar{T}_w - \bar{T}_\infty}, \quad C = \frac{\bar{C} - \bar{C}_\infty}{\bar{C}_w - \bar{C}_\infty},$$

$$Gr = \frac{\upsilon g\beta(\bar{T}_w - \bar{T}_\infty)}{U_0 v_0^2}, \quad Gm = \frac{\upsilon g\bar{\beta}(\bar{C}_w - \bar{C}_\infty)}{U_0 v_0^2}, \quad M = \sigma B_0^2\upsilon / \rho V_0^2,$$

$$Pr = \frac{\mu C_P}{\kappa}, \quad Sc = \upsilon/D, \quad U_P = \frac{\bar{u}_P}{U_0}, \quad R^2 = \frac{\alpha^2(\bar{T}_w - \bar{T}_\infty)}{\rho C_P \kappa U_0^2}, \tag{10}$$

where all variables are again defined in the notation section. Implementing these dimensionless variables in addition to equations (4) and (7) to (9), the governing conservation equations (2), (3) and (5) may be shown to take the following non-dimensional form:

$$\frac{\partial u}{\partial t} - (1 + \varepsilon A e^{nt})\frac{\partial u}{\partial y} = \frac{dU_\infty}{\partial t} + \frac{\partial^2 u}{\partial y^2} + Gr\theta + GmC + M(U_\infty - u), \tag{11}$$

$$\frac{\partial \theta}{\partial t} - (1 + \varepsilon A e^{nt})\frac{\partial \theta}{\partial y} = \frac{1}{Pr}\left[\frac{\partial^2 \theta}{\partial y^2} - R^2\right] + Ec\left(\frac{\partial u}{\partial y}\right)^2, \tag{12}$$

$$\frac{\partial C}{\partial t} - (1 + \varepsilon A e^{nt})\frac{\partial C}{\partial y} = \frac{1}{Sc}\frac{\partial^2 C}{\partial y^2}. \tag{13}$$

In due course the boundary conditions are also transformed to:

$$\left.\begin{aligned} &u = U_P, \quad \theta = 1 + \varepsilon e^{nt}, \quad C = 1 + \varepsilon e^{nt} \text{ on } y = 0, \\ &u \to U_\infty = 1 + \varepsilon e^{nt}, \quad \theta \to 0, \quad \Phi \to 0 \text{ as } y \to \infty. \end{aligned}\right\} \tag{14}$$

The system comprising (11) to (13) is well-posed and can yield either semi-analytical or numerical solutions. We elect to seek perturbation solutions here.

3. Solution Methodology

The two-point boundary value problem defined by equations (11) to (13) is non-linear and coupled. We adopt a perturbative series expansion about ε, $(\varepsilon << 1)$. As a first step to the solution of equations (11) to (13), we assume that:

$$f(y, t) = f_0(y) + \varepsilon e^{nt} f_1(y) + \cdots + \cdots, \tag{15}$$

where f stands for u, θ or Φ, i.e., f denotes a general dependent physical non-dimensional variable. Substituting (15) in (11) to (13), we find that the leading approximations satisfy the following sequence of equations:

$$\theta_0'' + Pr\theta_0' - R\theta_0 = -PrEc(u_0')^2, \tag{16}$$

$$\theta_1'' + Pr\theta_1' - (R + nPr)\theta_1 = -APr\theta_0' - 2PrEcu_0'u_1', \tag{17}$$

$$u_0'' + u_0' - Mu_0 = -M - Gr\theta_0 - Gm\Phi_0, \tag{18}$$

$$u_1'' + u_1' - (M + n)u_1 = -(M + n) - Gr\theta_1 - Gm\Phi_1 - Au_0', \tag{19}$$

$$\Phi_0'' + Sc\Phi_0' = 0, \tag{20}$$

$$\Phi_1'' + Sc\Phi_1' - nSc\Phi_1 = -ASc\Phi_0', \tag{21}$$

where prime denotes differentiation w.r.t. y. The corresponding boundary conditions now are:

$$\left.\begin{array}{l} u_0 = U_P,\ \ u_1 = 0,\ \ \theta_0 = 1,\ \ \theta_1 = 1,\ \ \Phi_0 = 1,\ \ \Phi_1 = 1 \text{ on } y = 0, \\ u_0 \to 1,\ \ u_1 \to 1,\ \ \theta_0 \to 0,\ \ \theta_1 \to 0,\ \ \Phi_0 \to 0,\ \ \Phi_1 \to 0 \text{ as } y \to \infty. \end{array}\right\} \tag{22}$$

The non-linear terms in equations (12), (16), (17) are multiplied by the Eckert number, Ec, in order to decouple them, since it is known that $Ec << 1$ for all incompressible fluids. We assume that:

$$\left.\begin{array}{l} u_0(y) = u_{00}(y) + Ec\, u_{01}(y),\ \ u_1(y) = u_{10}(y) + Ecu_{11}(y), \\ \theta_0(y) = \theta_{00}(y) + Ec\theta_{01}(y),\ \ \theta_1(y) = \theta_{10}(y) + Ec\theta_{11}(y), \\ \Phi_0(y) = \Phi_{00}(y) + Ec\Phi_{01}(y),\ \ \Phi_1(y) = \Phi_{10}(y) + Ec\Phi_{11}(y). \end{array}\right\} \tag{23}$$

Substituting equations (23) into the equations (16) to (21), we arrive at:

$$\theta_{00}'' + Pr\theta_{00}' - R^2\theta_{00} = 0, \tag{24}$$

$$\theta''_{01} + Pr\theta'_{01} - R^2\theta_{01} = -Pr(u'_{00})^2, \tag{25}$$

$$\theta''_{10} + Pr\theta'_{10} - nPr\theta_{10} = -APr\theta'_{00}, \tag{26}$$

$$\theta''_{11} + Pr\theta'_{11} - (R^2 + nPr)\theta_{11} = -APr\theta'_{01} - 2Pru'_{00}u'_{10}, \tag{27}$$

$$u''_{00} + u'_{00} - Mu_{00} = -Gr\theta_{00} - Gc\Phi_{00}, \tag{28}$$

$$u''_{01} + u'_{01} - Mu_{01} = -Gr\theta_{01} - Gc\Phi_{01}, \tag{29}$$

$$u''_{10} + u'_{10} - (M + n)u_{10} = -(M + n) - Gr\theta_{10} - Gm\Phi_{10} - Au'_{00}, \tag{30}$$

$$u''_{11} + u'_{11} - (M + n)u_{11} = -Gr\theta_{11} - Gm\Phi_{11} - Au'_{01}, \tag{31}$$

$$\Phi''_{00} + Sc\Phi'_{00} = 0, \tag{32}$$

$$\Phi''_{01} + Sc\Phi'_{01} = 0, \tag{33}$$

$$\Phi''_{10} + Sc\Phi'_{10} - nSc\Phi_{10} = ASc\Phi'_{00}, \tag{34}$$

$$\Phi''_{11} + Sc\Phi'_{11} - nSc\Phi_{11} = ASc\Phi'_{01}. \tag{35}$$

Equations (24) to (35) are to be solved subject to the corresponding boundary conditions:

$$\left.\begin{array}{l} u_{00} = U_P, \;\; u_{01} = u_{10} = u_{11} = 0, \;\; \theta_{00} = 1, \;\; \theta_{10} = 1, \;\; \theta_{01} = \theta_{11} = 0, \\ \qquad \Phi_{00} = 1, \;\; \Phi_{10} = 1, \;\; \Phi_{01} = \Phi_{11} = 0 \text{ on } y = 0, \\ u_{00} = 1, \;\; u_{01} = u_{10} = u_{11} = 0, \;\; \theta_{00} = \theta_{10} = \theta_{01} = \theta_{11} = 0, \\ \qquad \Phi_{00} = \Phi_{10} = \Phi_{01} = \Phi_{11} = 0 \text{ as } y \to 0. \end{array}\right\} \tag{36}$$

The solutions of the equations (24) to (35) under the boundary the conditions (36) are:

$$\theta_{00}(y) = e^{-m_2 y}, \tag{37}$$

$$\Phi_{00}(y) = e^{-Scy}, \tag{38}$$

$$\Phi_{01}(y) = 0, \tag{39}$$

$$\Phi_{10}(y) = \left(1 + \frac{ASc}{n}\right)e^{-m_1 y} - \frac{ASc}{n}e^{-Sc\, y}, \tag{40}$$

$$\Phi_{11}(y) = 0, \tag{41}$$

$$u_{00}(y) = 1 + H_3 e^{-m_3 y} + H_1 e^{-m_2 y} + H_2 e^{-Scy}, \tag{42}$$

$$\left.\begin{aligned} \theta_{01}(y) = {} & q_7 e^{-m_2 y} + q_1 e^{-2m_3 y} + q_2 e^{-2m_2 y} + q_3 e^{-2Scy} + q_4 e^{-(m_2+m_3)y} \\ & + q_5 e^{-(m_2+Sc)y} + q_6 e^{-(m_3+Sc)y}, \end{aligned}\right\} \tag{43}$$

$$\left.\begin{aligned} u_{01}(y) = {} & H_{11} e^{-m_3 y} + H_4 e^{-m_2 y} + H_5 e^{-2m_3 y} + H_6 e^{-2m_2 y} + H_7 e^{-2Scy} \\ & + H_8 e^{-(m_2+m_3)y} + H_9 e^{-(m_2+Sc)y} + H_{10} e^{-(m_3+Sc)y}, \end{aligned}\right\} \tag{44}$$

$$\theta_{10}(y) = D_2 e^{-m_4 y} + D_1 e^{-m_2 y}, \tag{45}$$

$$\left.\begin{aligned} u_{10}(y) = {} & H_{17} e^{-m_5 y} + H_{12} e^{-m_3 y} + H_{13} e^{-m_2 y} + H_{14} e^{-Scy} \\ & + H_{15} e^{-m_1 y} + H_{16} e^{-m_4 y}, \end{aligned}\right\} \tag{46}$$

$$\left.\begin{aligned} \theta_{11}(y) = {} & q_{24} e^{-m_4 y} + q_8 e^{-m_2 y} + q_9 e^{-2m_3 y} + q_{10} e^{-2Scy} + q_{11} e^{-(m_2+m_3)y} \\ & + q_{12} e^{-(m_2+Sc)y} + q_{13} e^{-(m_3+Sc)y} + q_{14} e^{-m_2 y} + q_{15} e^{-(m_2+m_4)y} \\ & + q_{16} e^{-(m_2+m_1)y} + q_{17} e^{-(m_2+m_5)y} + q_{18} e^{-(m_4+Sc)y} + q_{19} e^{-(m_1+Sc)y} \\ & + q_{20} e^{-(m_5+Sc)y} + q_{21} e^{-(m_3+m_4)y} + q_{22} e^{-(m_1+m_3)y} + q_{23} e^{-(m_3+m_5)y}, \end{aligned}\right\} \tag{47}$$

$$\left.\begin{aligned} u_{11}(y) = {} & H_{35} e^{-m_5 y} + H_{18} e^{-m_3 y} + H_{19} e^{-m_2 y} + H_{20} e^{-2m_3 y} + H_{21} e^{-2m_2 y} \\ & + H_{22} e^{-2Scy} + H_{23} e^{-(m_2+m_3)y} + H_{24} e^{-(m_2+Sc)y} \\ & + H_{25} e^{-(m_5+Sc)y} + H_{26} e^{-(m_2+m_4)y} + H_{27} e^{-(m_2+m_3)y} \\ & + H_{28} e^{-(Sc+m_4)y} + H_{29} e^{-(Sc+m_1)y} + H_{30} e^{-(Sc+m_5)y} \\ & + H_{31} e^{-(m_3+m_4)y} H_{32} e^{-(m_3+m_1)y} + H_{33} e^{-(m_3+m_2)y} \\ & + H_{34} e^{-m_4 y}. \end{aligned}\right\} \tag{48}$$

4. Skin-friction

Knowing the velocity field, the skin-friction coefficient can be obtained in non-dimensional form, and is given by:

$$\tau = \frac{\bar{\tau}}{\rho U_0 v_0} = \left.\frac{\partial u}{\partial y}\right|_{y=0} = \left.\frac{\partial u_0}{\partial y} + \varepsilon e^{nt}\frac{\partial u_1}{\partial y}\right|_{y=0}$$

$$\left.\begin{aligned}
&= -m_3H_3 - m_2H_1 - ScH_2 + Ec[-m_3H_{11} - m_2H_4 - 2m_3H_5 - 2m_2H_6 - 2ScH_7 \\
&-(m_2+m_3)H_8 - (m_2+Sc)H_9 - (m_3+Sc)H_{10}] + \varepsilon e^{nt}[\{m_5H_{17} - m_3H_{12} - m_2H_{13} \\
&-ScH_{14} - m_1H_{15} - m_4H_{16}\} + Ec\{-m_5H_{35} - m_3H_{18} - m_2H_{19} - 2m_3H_{20} - 2m_2H_{21} \\
&-2ScH_{22} - (m_2+m_3)H_{23} - (m_2+Sc)H_{24} - (m_5+Sc)H_{25} - (m_2+m_4)H_{26} \\
&-(m_2+m_3)H_{27} - (m_4+Sc)H_{28} - (m_2+Sc)H_{29} - (m_5+Sc)H_{30} - (m_3+m_4)H_{31} \\
&-(m_2+m_1)H_{32} - (m_2+m_3)H_{33} - m_4H_{34}\}].
\end{aligned}\right\} \tag{49}$$

This allows the computation of drag effects at the plate, a characteristic of considerable importance in materials processing.

5. Heat Transfer

Evaluation of the temperature field similarly allows the calculation of the heat transfer rate at the plate, which is in the non-dimensional form computable as the Nusselt number:

$$Nu = \frac{-x}{(\bar{T}_w + \bar{T}_\infty)}\left(\frac{\partial \bar{T}}{\partial \bar{y}}\right)_{\bar{y}=0} \Rightarrow NuRe_x^{-1} = -\left.\frac{\partial \theta}{\partial y}\right|_{y=0} = -\left(\frac{\partial \theta_0}{\partial y} + \varepsilon e^{nt}\frac{\partial \theta_1}{\partial y}\right)_{y=0}$$

$$\left.\begin{aligned}
&= -[-m_2 + Ec\{-m_2q_7 - 2m_3q_1 - 2m_2q_2 - 2Scq_3 - (m_2+m_3)q_4 - (m_2+Sc)q_5 \\
&-(m_3+Sc)q_6\} + \varepsilon e^{nt}[\{-D_2m_4 - D_1m_2\} + Ec\{-m_4q_{24} - m_2q_8 - 2m_3q_9 - 2Scq_{10} \\
&-(m_2+m_3)q_{11} - (Sc+m_2)q_{12} - (Sc+m_3)q_{13} - 2m_2q_{14} - (m_2+m_4)q_{15} \\
&-(m_1+m_2)q_{16} - (m_2+m_5)q_{17} - (m_4+Sc)H_{18} - (m_1+Sc)H_{19} - (m_5+Sc)H_{20} \\
&-(m_3+m_4)q_{21} - (m_1+m_3)q_{22} - (m_3+m_5)q_{23}\}]],
\end{aligned}\right\} \tag{50}$$

where $Re_x = \frac{V_0 x}{\upsilon}$ is the local Reynolds number.

6. Mass (Species) Transfer

Finally the concentration field can be used to determine the rate of mass transfer coefficient at the plate surface which in non-dimensional form is calculated using the Sherwood number:

$$Sh = \frac{-x}{(\overline{C}_w - \overline{C}_\infty)}\left(\frac{\partial \overline{C}}{\partial \overline{y}}\right)_{\overline{y}=0} \Rightarrow ShRe_x^{-1} = -\left.\frac{\partial C}{\partial y}\right|_{y=0} = -\left(\frac{\partial C_0}{\partial y} + \varepsilon e^{nt}\frac{\partial C_1}{\partial y}\right)_{y=0}$$

$$= -\left[-Sc + \varepsilon e^{nt}\left\{-m_1\left(1 + \frac{ASc}{n}\right) + ASc^2\right\}\right]. \tag{51}$$

7. Graphical Results and Discussion

Selected computations have been depicted graphically in Figures 1 to 12. The figures presented generally show the spatial variable distribution at a fixed time, t. All data corresponding to each figure is included therein. $Gm = Gr = 5$ implies strong species and thermal buoyancy forces; $Sc = 0.6$ approximately simulates lower molecular weight gases diffusing in air. $R^2 = \frac{\alpha^2(\overline{T}_w - \overline{T}_\infty)}{\rho C_P \kappa U_0^2}$ is fixed as 0.5 unless otherwise stated. $Pr = 0.71$ which represents air. The current perturbative series method has been well-validated in previous studies by Ahmed [34, 35] and therefore comparisons with earlier studies are omitted here for brevity. Also we have excluded species transfer distributions also for conservation of space.

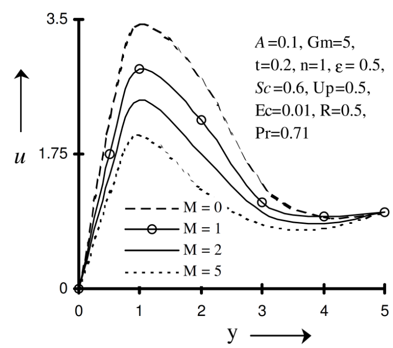

Figure 1. Effects of magnetic parameter on flow velocity.

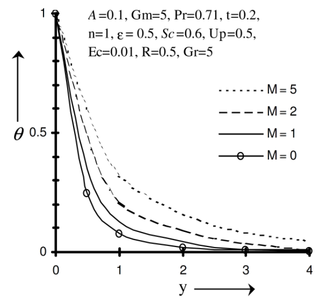

Figure 2. Effects of magnetic parameter on temperature.

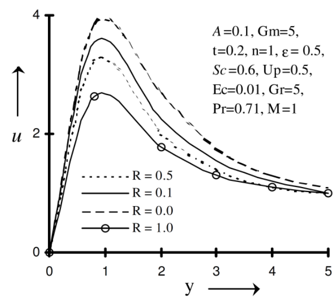

Figure 3. Effects of thermal radiation on flow velocity.

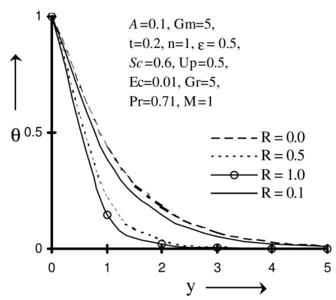

Figure 4. Effects of thermal radiation on temperature.

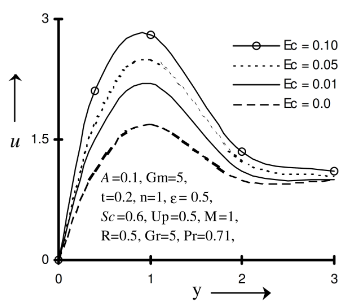

Figure 5. Effects of viscous dissipation on flow velocity.

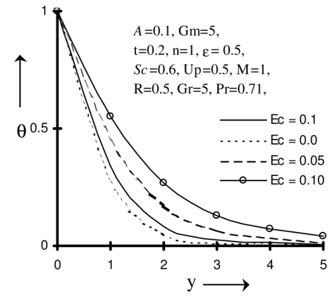

Figure 6. Effects of viscous dissipation on temperature.

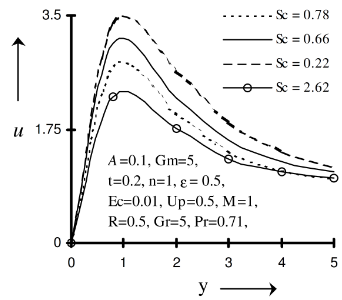

Figure 7. Effects of Schmidt number on flow velocity.

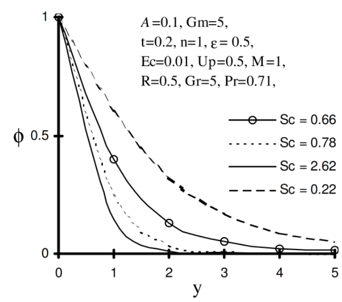

Figure 8. Effects of Schmidt number on temperature.

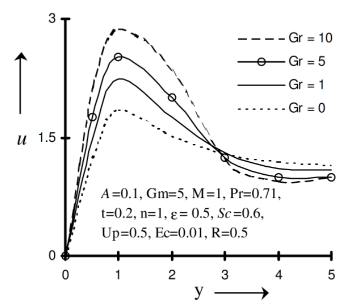

Figure 9. Effects of Grashof number on flow velocity.

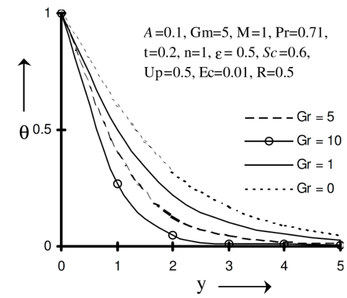

Figure 10. Effects of Grashof number on temperature.

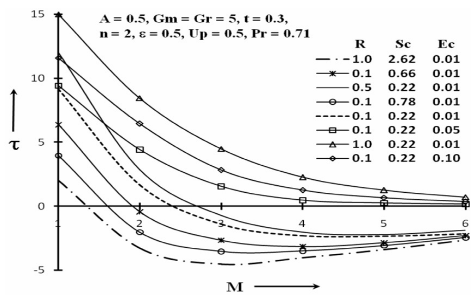

Figure 11. Skin-friction coefficient versus Hartmann number for various values of *R*, *Sc* and *Ec*.

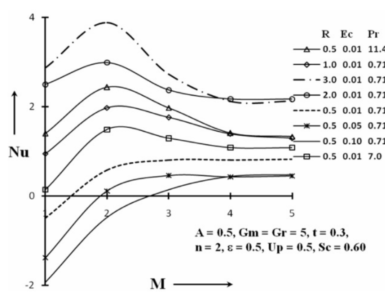

Figure 12. Nusselt number versus Hartmann number for various R, Ec and *Pr*.

Figure 1 shows the velocity response (*u*) with transverse coordinate (*y*) for various magnetohydrodynamic body force parameters (*M*). In the dimensionless momentum equation (11) the magnetic effect appears as the Lorentzian linear body force term, $+M(U_\infty - u)$. This acts perpendicular to the plate and effectively retards the boundary layer flow along the plate length. This is indeed the trend observed in Figure 1 where a strong deceleration in the flow is achieved with an increase in *M* from 0 (non-conducting case, i.e., Lorentz force vanishes) through 1, 2, to 5. In no case, however, is there flow reversal, i.e., velocities remain positive through the boundary layer.

Figure 2 shows the dimensionless temperature distribution (θ) with various magnetic parameters (M). The trend is very consistent for all M values, i.e., a monotonic decay from a maximum at the wall to the free stream. Temperatures are strongly enhanced with increasing magnetic field. The supplementary work exerted by the fluid in dragging against the magnetic field retarding action, is dissipated as thermal energy which serves to heat the fluid. These results concur with many studies on magnetohydrodynamic free convection boundary layer flows, for example, by Char [14], Shateyi and Petersen [23], Ogulu and Prakash [24], Chamkha [37] and Cramer and Pai [38].

Figure 3 depicts the spatial velocity distribution with various radiation parameters (R). The trend is similar to that for the velocity response to different M values, i.e., a peak arises close to the wall and then all profiles decay smoothly to unity as prescribed by the free stream boundary condition. The radiation parameter arises only in the energy equation (12) in the thermal diffusion term, $\frac{1}{Pr}\left[\frac{\partial^2\theta}{\partial y^2} - R^2\right]$, and via coupling of the temperature field (θ) with the buoyancy terms in the momentum equation (11), the velocity field is indirectly influenced by thermal radiation effects. $R^2 = \frac{\alpha^2(\overline{T}_w - \overline{T}_\infty)}{\rho C_P \kappa U_0^2}$ and therefore for $R = 0$, radiation effects vanish and increase for $R > 0$. An increase in R clearly reduces substantially the velocity in the boundary layer, i.e., decelerates the flow. Similarly in Figure 4, the temperature θ is reduced in this regime with increasing thermal radiation. For $R = 1$, thermal radiation and thermal conduction contributions are equivalent. For $R > 1$, thermal radiation is dominant over conduction and vice versa for $R < 1$.

Figures 5 and 6 illustrate the variation of velocity and temperature with various Eckert numbers (Ec). Ec quantifies the ratio of kinetic energy of the flow to the enthalpy difference. Velocity is noticeably enhanced with an increase in Ec, as seen in Figure 5. No flow reversal has been computed in our case although such an effect has been reported for the case of a moving wall by Gschwendtner [39] who studied much higher values of Ec. Conversely in Figure 6, temperature is strongly increased with a rise in Ec. With increasing viscous heating, mechanical energy is converted into thermal energy in the flow which heats the fluid. Eckert number effectively signifies the difference between the total mechanical power input and the smaller amount of total power input which produces thermodynamically reversible effects, i.e., elevations in kinetic and potential energy. This difference constitutes the energy dissipated as thermal energy by viscous effects, i.e., work done by the viscous fluid in overcoming internal friction, hence the term viscous heating. Positive values of Ec correspond to plate cooling, i.e., loss of heat from the plate to the fluid; negative values imply the reverse, i.e., plate heating wherein heat is received by the plate from the fluid. In the present study, we have restricted attention to the former case. Also we note that increasing Ec causes an increase in Joule heating as the magnetic field adds energy to the fluid boundary layer due to the work done in dragging the fluid, although this effect has been neglected in the present study.

Figures 7 and 8 present the spatial velocity and species concentration profiles for various Schmidt numbers (Sc), again at $t = 0.2$. Sc quantifies the relative effectiveness of momentum and mass transport by diffusion. Higher values of Sc amount to a fall in the chemical molecular diffusivity, i.e., less diffusion therefore takes place by species transfer. In the present study we have performed calculations for Prandtl number $Pr = 0.7$, so that $Pr \neq Sc$. Physically, this implies that the thermal and species diffusion regions are of different extents. An increase in Sc will suppress concentration in the boundary layer regime. Higher Sc will imply a decrease of molecular diffusivity causing a reduction in concentration boundary layer thickness. Lower Sc will result in higher concentrations, i.e., greater molecular (species) diffusivity causing an increase in concentration boundary layer thickness. For $Sc = 1.0$, the momentum and concentration boundary layer thicknesses are of the same value approximately, i.e., both species and momentum will diffuse at the same rate in the boundary layer. Velocity, u, as shown in Figure 7 is found to decrease strongly with an increase in Schmidt number from 0.22 (hydrogen diffusing in air), 0.66 and 0.78 (in all these cases species diffusivity $>$ momentum diffusivity) through to 2.62 (species diffusivity $<$ momentum diffusivity). Similarly there is a strong reduction in species concentration values (Φ) as shown in Figure 8 with a rise in Sc. Concentration profiles follow a smooth decay from the wall (plate) to the edge of the boundary layer; velocity profiles, however, as in earlier graphs peak close to the plate and then descend thereafter towards the free stream.

Figures 9 and 10 show the effect of thermal buoyancy parameter (Gr) on the velocity and temperature profiles, respectively. For the case of $Gr = 0$, thermal buoyancy vanishes. For $Gr > 0$, it is present. A strong acceleration in the flow is induced with a rise in Gr from 0 through 1 (thermal buoyancy and viscous forces equivalent) to 5 and 10 (for which thermal buoyancy forces exceed viscous hydrodynamic forces in the boundary layer). This pattern is sustained for some distance into the boundary layer, transverse to the plate; however, as we approach the free stream, a reverse in this trend is witnessed with increasing thermal buoyancy serving to damp the flow, i.e., decelerate the boundary layer flow. Conversely there is a consistent suppression of temperatures with a rise in Gr, as observed in Figure 10. The maximum temperatures correspond to $Gr = 0$, i.e., the case of pure forced convection heat transfer.

In Figure 11, the distribution of skin friction coefficient with magnetic parameter (Hartmann number, M) is shown at $t = 0.3$ with various R, Sc and Ec values. Inspection shows that increasing radiation decelerates the flow, i.e., reduces skin friction, to the extent that for $R = 1.0$, flow reversal is observed, i.e., skin friction becomes negative. Clearly all profiles decay as M increases since larger Hartmann number corresponds to greater magnetohydrodynamic drag which decelerates the flow. An increase in Sc also strongly reduces the skin friction, in consistency with earlier discussion for the velocity response (Figure 7). $Sc = 2.62$ (maximum value studied) could correspond realistically to ethyl benzene (i.e., heavier molecular weight hydrocarbon gases) diffusing in air. Increasing Ec is found also to decrease skin friction. Finally in Figure 12, we observe that an increase in Prandtl number (Pr) which signifies the ratio of momentum to thermal diffusivity generally decreases heat transfer rate at the wall, i.e., Nusselt number. Nusselt number, however, is increased with Hartmann number (magnetic parameter) although for very high $Pr\ (= 11.4)$, there is a subsequent plummet in Nu value with further increase in M. Increasing radiation parameter, R, tends to boost the heat transfer rate at the wall, i.e., elevates Nu magnitudes. For low Pr values however with $R = 0.5$, there are negative Nu values induced at the wall. With rising Ec values, the Nu values are generally decreased, to the point of becoming increasingly negative for $Ec = 0.1$. We note that in all cases $A > 0$ in our computations indicating uniform suction at the wall.

8. Conclusions

Perturbation series solutions have been obtained to study the influence of thermal radiation and viscous heating on transient convective heat and mass transfer in boundary layer flow from an upward translating plate. A flux model has been employed to simulate thermal radiation effects. A range of Schmidt numbers have also been investigated to simulate the diffusion of various species in air including hydrogen, oxygen and ethyl benzene. The analysis has shown that increasing thermal buoyancy effects (simulated via thermal Grashof number) accelerate the flow but depress temperatures. Increasing thermal radiation acts to generally boost Nusselt number values at the plate, whereas increasing Eckert number (viscous dissipation parameter) effectively reduces heat transfer rates at the wall and also skin friction, i.e., wall shear stress values. The present study has been confined to Newtonian flow. Future investigations will consider viscoelastic and power-law rheological fluid models and will be communicated in the near future.

9. Nomenclature

$(\bar{u}, \bar{v})$	Dimensional velocity components along the $\bar{x}$, $\bar{y}$ directions $(\mathrm{m/s})$,
$\bar{T}$	Dimensional temperature of the fluid (K),
$\bar{T}_w$	Dimensional temperature at the plate (K),
$\bar{T}_\infty$	Dimensional fluid temperature in the free stream (K),
$\bar{C}$	Dimensional species concentration $(\mathrm{Kg.m^{-3}})$,
$\bar{C}_w$	Dimensional species concentration at the plate $(\mathrm{Kg.m^{-3}})$,
$\bar{C}_\infty$	Dimensional species concentration in the free stream $(\mathrm{Kg.m^{-3}})$,
$\bar{q}$	Radiative heat flux,
g	Gravity $(\mathrm{m/s^2})$,
$\bar{\tau}_x$	Dimensional shear stress $(\mathrm{N.m^{-2}})$,
v_0	Suction velocity $(\mathrm{m/s})$,
C_P	Specific heat at constant pressure $(\mathrm{J.kg^{-1}.K})$,
Pr	Prandtl number,
R	Radiation parameter,

A	Suction parameter,
Sc	Schmidt number,
D	Mass diffusion coefficient $(\mathrm{m}^2.\mathrm{s}^{-1})$,
t	Time (S),
Gr	Thermal Grashof number,
Gm	Mass Grashof number,
B_0	Magnetic field flux density,
M	Hartmann number.

Greek Symbols

α	Thermal diffusivity $(\mathrm{m}^2.\mathrm{s}^{-1})$,
β	Coefficient of thermal expansion (K^{-1}),
$\overline{\beta}$	Coefficient of thermal expansion with concentration (K^{-1}),
θ	Dimensionless temperature (K),
Φ	Dimensionless species concentration $(\mathrm{kg.m}^{-3})$,
κ	Thermal conductivity $(\mathrm{W.m}^{-1}.\mathrm{K}^{-1})$,
ρ	Density $(\mathrm{kg.m}^{-3})$,
μ	Coefficient of viscosity $(\mathrm{kg.s}^{-1}\mathrm{m})$,
υ	Kinematic viscosity $(\mathrm{m}^2.\mathrm{s}^{-1})$,
ω	Frequency parameter (s^{-1}),
τ	Dimensional shearing stress $(\mathrm{N.m}^{-2})$,
σ	Electrical conductivity $(\mathrm{S/m})$.

Subscripts

w	Evaluated at wall conditions,
∞	Evaluated at free stream conditions.

10. Appendix

$$m_1 = [Sc + \sqrt{Sc^2 + 4nSc^2}\,]/2, \quad m_2 = [Pr + \sqrt{Pr^2 + 4R^2}\,]/2,$$

$$H_1 = \frac{Gr}{Pr(Pr-1) - M}, \quad m_3 = [1 + \sqrt{1 + 4M}\,]/2,$$

$$m_4 = [Pr + \sqrt{Pr^2 + 4(R^2 + nPr)}\,]/2, \quad H_2 = \frac{-Gm}{Sc(Sc-1) - M},$$

$$H_3 = 1 - U_P + H_1 + H_2, \quad H_4 = \frac{-Grq_7}{m_2^2 - m_2 - M}, \quad H_5 = \frac{-q_1 Gr}{4m_3^2 - m_3 - M},$$

$$H_6 = \frac{-q_2 Gr}{4m_2^2 - m_2 - M}, \quad H_7 = \frac{-q_3 Gr}{4Sc^2 - Sc - M},$$

$$H_8 = \frac{-q_4 Gr}{(m_2 + m_3)^2 - (m_2 + m_3 + M)}, \quad H_9 = \frac{-q_5 Gr}{(m_2 + Sc)^2 - (m_2 + Sc + M)},$$

$$H_{10} = \frac{-q_6 Gr}{(m_3 + Sc)^2 - (m_3 + Sc + M)}, \quad H_{11} = \frac{-q_1 Gr}{4Pr^2 - 2Pr - M},$$

and the other parameters are not presented here to conserve space.

References

[1] J. Szekely and C. W. Chang, Electromagnetically driven flows in metals processing, J. Metals 28 (1976), 6-11.

[2] H. Yasuda, Applications of high magnetic fields in materials processing, Fluid Mech. Appl. 80 (2007), 329-344.

[3] H. B. Lofgren and H. O. Akerstedt, Damping mechanisms of perturbations in electromagnetically-braked horizontal film flows, Fluid Dyn. Res. 26 (2000), 53-68.

[4] P. A. Davidson, Magnetohydrodynamics in materials processing, Ann. Rev. Fluid Mech. 31 (1999), 273-300.

[5] A. E. Organ and N. Riley, Magnetohydrodynamic boundary layers in Czochralski crystal growth, IMA J. Appl. Math. 36 (1986), 117-128.

[6] B. Gebhart et al., Buoyancy-induced Flows and Transport, Hemisphere Press, Washington DC, USA, 1988.

[7] V. M. Soundalgekar, Free convection effects on steady MHD flow past a vertical porous plate, J. Fluid Mech. 66 (1974), 541-551.

[8] D. V. Krishna and D. R. V. Prasada Rao, Hydromagnetic Ekman layer over an oscillatory porous plate, Indian J. Pure Appl. Math. 11(9) (1980), 1225-1234.

[9] M. A. Hossain and A. C. Mandal, Unsteady hydromagnetic free convection flow past an accelerated infinite vertical porous plate, Astrophysics and Space Science 111(1) (1985), 87-95.

[10] N. G. Kafoussias, MHD thermal-diffusion effects on free-convective and mass-transfer flow over an infinite vertical moving plate, Astrophysics and Space Science 192(1) (1992), 11-19.

[11] M. A. Sattar, Unsteady hydromagnetic free convection flow with hall current mass transfer and variable suction through a porous medium near an infinite vertical porous plate with constant heat flux, Int. J. Energy Research 18(9) (1994), 771-775.

[12] M. Acharya, G. C. Dash and L. P. Singh, Effect of chemical and thermal diffusion with Hall current on unsteady hydromagnetic flow near an infinite vertical porous plate, J. Phys. D: Appl. Phys. 28 (1995), 2455-2464.

[13] N. D. Nanousis, The unsteady hydromagnetic thermal boundary layer with suction, Mech. Res. Comm. 23(1) (1996), 81-90.

[14] M. I. Char, Heat and mass transfer in a hydromagnetic flow of the viscoelastic fluid over a stretching sheet, J. Math. Anal. Appl. 186 (1994), 674-689.

[15] S. Rawat, R. Bhargava, Renu Bhargava and O. Anwar Bég, Transient magnetomicropolar free convection heat and mass transfer through a non-Darcy porous medium channel with variable thermal conductivity and heat source effects, Proc. IMechE Part C: J. Mechanical Engineering Science 223 (2009), 2341-2355.

[16] J. Zueco, O. Anwar Bég, H. S. Takhar and V. R. Prasad, Thermophoretic hydromagnetic dissipative heat and mass transfer with lateral mass flux, heat source, Ohmic heating and thermal conductivity effects: network simulation numerical study, Applied Thermal Engineering 29 (2009), 2808-2815.

[17] A. J. Nowak et al., Coupling of conductive, convective and radiative heat transfer in Czochralski crystal growth process, Computational Materials Science 25 (2002), 570-576.

[18] S. Mazumder and A. Kersch, A fast Monte Carlo scheme for thermal radiation in semiconductor processing applications, Numerical Heat Transfer Part B: Fundamentals 37 (2000), 185-199.

[19] G. K. Malikov, D. L. Lobanov, K. Y. Malikov, V. G. Lisienko, R. Viskanta and A. G. Fedorov, Direct flame impingement heating for rapid thermal materials processing, Int. J. Heat and Mass Transfer 44 (2001), 1751-1758.

[20] A. G. Fedorov, K. H. Lee and R. Viskanta, Inverse optimal design of the radiant heating in materials processing and manufacturing, J. Materials Engineering and Performance 7 (1998), 719-726.

[21] F. T. Lentes and N. Siedow, Three-dimensional radiative heat transfer in glass cooling processes, Glass Sci. Technol.: Glastechnische Berichte 72(6) (1999), 188-196.

[22] M. F. Modest, Radiation Heat Transfer, MacGraw-Hill, New York, 1992.

[23] S. Shateyi and Mark Petersen, Thermal radiation and buoyancy effects on heat and mass transfer over a semi-infinite stretching surface with suction and blowing, J. Appl. Math.10 (2008), 1-12.

[24] A. Ogulu and J. Prakash, Heat transfer to unsteady magneto-hydrodynamic flow past an infinite moving vertical plate with variable suction, Physica Scripta 74 (2006), 232-239.

[25] Mostafa Abd El-Hameed Mahmoud, Slip effects on flow and heat transfer of a non-Newtonian fluid on a stretching surface with thermal radiation, Int. J. Chemical Reactor Engineering 6 (2008), A92-A97.

[26] S. Shateyi and S. S. Motsa, Thermal radiation effects on heat and mass transfer over an unsteady stretching surface, Mathematical Problems in Engineering 10 (2009), 1-13.

[27] I. Muhaimin, R. Kandasamy and I. Hashim, Thermophoresis and chemical reaction effects on MHD mixed convective heat and mass transfer past a porous wedge with variable viscosity in the presence of viscous dissipation, Int. J. Computational Methods in Engineering Science and Mechanics 10 (2009), 231-240.

[28] N. S. Elgazery and M. A. Hassan, Numerical study of radiation effect on MHD transient mixed-convection flow over a moving vertical cylinder with constant heat flux, Comm. Numer. Meth. Engrg. 24 (2008), 1183-1202.

[29] Z. Abbas and T. Hayat, Radiation effects on MHD flow in a porous space, Int. J. Heat Mass Transfer 51 (2008), 1024-1033.

[30] M. G. Reddy and N. Bhaskar Reddy, Radiation and mass transfer effects on unsteady MHD free convection flow of an incompressible viscous fluid past a moving vertical cylinder, Theo. Appl. Mech. 36(3) (2006), 239-260.

[31] V. R. Prasad and N. Bhaskar Reddy, Radiation and mass transfer effects on an unsteady MHD free convection flow past a heated vertical plate in a porous medium with viscous dissipation, Theo. Appl. Mech. 34 (2007), 135-160.

[32] L. Kumar, Finite element analysis of combined heat and mass transfer in hydromagnetic micropolar flow along a stretching sheet, Computational Materials Science 46 (2009), 841-848.

[33] O. Anwar Bég, J. Zueco, T. A. Bég, H. S. Takhar and E. Kahya, NSM analysis of timedependent nonlinear buoyancy-driven double-diffusive radiative convection flow in non-Darcy geological porous media, Acta Mechanica 202 (2009), 181-204.

[34] S. Ahmed, Transient 3-D flow through a porous medium with transverse permeability oscillating with time, Emirates J. Engineering Res. 13 (2008), 11-17.

[35] S. Ahmed, Free and forced convective three-dimensional flow with heat and mass transfer, Int. J. Appl. Math. Mech. 2(1) (2008), 26-38.

[36] S. Shateyi, P. Sibanda and S. S. Motsa, Magnetohydrodynamic flow past a vertical plate with radiative heat transfer, ASME J. Heat Transfer 129(12) (2007), 1708-1713.

[37] A. J. Chamkha, Thermal radiation and buoyancy effects on hydromagnetic flow over an accelerated permeable surface with heat source and sink, Int. J. Engineering Science 38(15) (2000), 1699-1712.

[38] K. C. Cramer and S. I. Pai, Magnetofluid Dynamics for Engineers and Applied Physicists, MacGraw-Hill, New York, 1973.

[39] M. A. Gschwendtner, The Eckert number phenomenon: Experimental investigations on the heat transfer from a moving wall in the case of a rotating cylinder, Heat Mass Transfer 40(6-7) (2004), 551-559.